analytical chemistry

pubs.acs.org/ac Article

Nitro Indole Derivatives as Novel Dual-Polarity Matrices for MALDI Mass Spectrometry and Imaging with Broad Applications

Qiaoli Liang,* Pritam Mondal, Qi Li, Tahir Maqbool, Chao Zhao, Daqian Jiang, Greg J. Szulczewski, and Gayan B. Wijeratne*

Cite This: *Anal. Chem.* 2024, 96, 1668−1677 Read Online

ACCESS | Metrics & More | Article Recommendations | Supporting Information

ABSTRACT: A new matrix framework is presented in this study for the improved ionization efficiency of complex mixtures by matrix-assisted laser desorption ionization (MALDI) mass spectrometry/imaging. Five nitro indole (NI) derivatives [3-methyl-4-nitro-1H-indole (3,4-MNI), 3-methyl-6-nitro-1H-indole (3,6-MNI), 2,3-dimethyl-4-nitro-1H-indole (2,3,4-DMNI), 2,3-dimethyl-6-nitro-1H-indole (2,3,6-DMNI), and 4-nitro-1H-indole (4-NI)] were synthesized and shown to produce both positive and negative ions with a broad class of analytes as MALDI matrices. NI matrices were compared to several common matrices, such as 2,5-dihydroxybenzoic acid (DHB), alpha-cyano-4-hydroxylcinnamic acid (CHCA), sinapinic acid (SA), 1,5-diaminonaphthelene (1,5-DAN), and 9-aminoacridine (9-AA), for the analysis of lipid, peptide, protein, glycan, and perfluorooctanesulfonic acid (PFOS) compounds. 3,4-MNI demonstrated the best performance among the NI matrices. This matrix resulted in reduced ion suppression and better detection sensitivity for complex mixtures, for example, egg lipids/milk proteins/PFOS in tap water, while 2,3,6-DMNI was the best matrix for blueberry tissue imaging. Several important aspects of this work are reported: (1) dual-polarity ion production with NI matrices and complex mixtures; (2) quantitative analysis of PFOS with a LOQ of 0.5 ppb in tap water and 0.05 ppb in MQ water (without solid phase extraction enrichment), with accuracy and precision within 5%; (3) MALDI imaging with 2,3,6-DMNI as a matrix for plant metabolite/lipid identification with ionization enhancement in the negative ion mode m/z 600−900 region; and (4) development of a thin film deposition under/above tissue method for MALDI imaging with a vacuum sublimation matrix on a high-vacuum MALDI instrument.

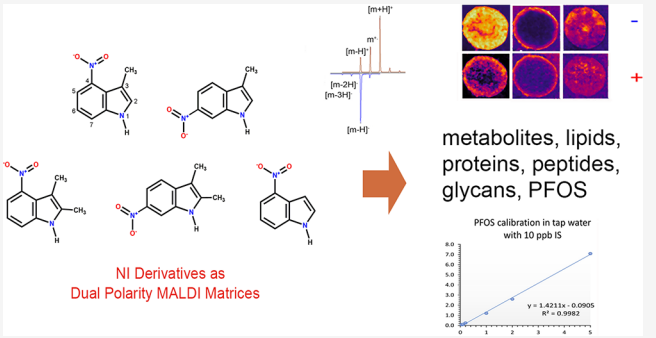

INTRODUCTION

Since its initial development in the 1980s,[1] Matrix-assisted laser desorption ionization mass spectrometry (MALDI MS) has been applied to identify/detect a wide range of natural or synthetic compounds, such as lipids,[2] peptides,[3] proteins,[4] glycans,[5] oligonucleotides,[6] and polymers.[7] MALDI matrix molecules absorb photons and transfer energy to the analyte and assist with analyte desorption and ionization.[8] Analytes are generally detected in positive ion mode as protonated, metal ion adducted, or radical cations, or in negative ion mode as deprotonated or radical anions.[9] Over the past few decades, a large number of matrix molecules have been identified to expand applications,[2,10] and discovery of matrix molecules with broad applications for both positive and negative ions has been an ongoing quest, to simplify matrix choices during sample preparation and enhance target molecule detection sensitivity in complex mixtures. Recent research on dual-polarity MALDI matrix molecules has focused on lipid analysis, as lipids are a diverse family of compounds, with some ionizing better in positive ion mode and some in negative ion mode.[2] Several aromatic amine compounds have been reported as dual-polarity matrices for lipid analysis, including 1,8-di(piperidinyl)-naphthalene (DPN),[11] nor-harmane,[12] 1,5-diaminonaphthalene (1,5-DAN),[13,14] 3-aminophthalhydrazide (luminol),[15] anthranilic derivative COOH-NHMe (IV),[16] and hydralazine.[17]

Indole is an electron-rich compound widely distributed in biological systems such as proteins (amino acid tryptophan side chain) and alkaloids.[18] Some existing indole-related MALDI matrices are trans-3-indoleacrylic acid (IAA) for polymers and steroids;[19−21] indole-3-pyruvic acid (IPA) for peptides and proteins;[22] and 9H-pyrido[3,4-b]-indole (nor-harmane) for lipids, proteins, peptides, carbohydrates, and synthetic polymers.[12,23−26] Nitro-containing matrices generally have a nitro group attached to a benzene ring, such as 9-nitroanthracene (9-NA) for polymers and organic ligands,[27,28] 2-nitrophlorogluci-

Received: October 17, 2023
Revised: December 13, 2023
Accepted: December 15, 2023
Published: January 16, 2024

https://doi.org/10.1021/acs.analchem.3c04684
Anal. Chem. 2024, 96, 1668−1677

nol (2-NPG) for protein multiple charging,[29] 5-nitrosalicylic acid (5-NSA) for glycan in source decay (ISD),[30] 3-hydroxy-4-nitrobenzoic acid (3H4NBA)/3-hydroxy-2-nitrobenzoic acid (3H2NBA) for peptide ISD,[31,32] and 4-nitroaniline (PNA) for lipids.[33] Nitro substituted β-carboline (nor-harmane) and carbazole derivatives were also reported.[34,35]

MALDI matrix development is of continual research interest with the aim to expand applications, improve analytical figures of merit, and identify new molecular architecture for matrix design. In this study, five indole derivatives [3-methyl-4-nitro-1H-indole (3,4-MNI), 3-methyl-6-nitro-1H-indole (3,6-MNI), 2,3-dimethyl-4-nitro-1H-indole (2,3,4-DMNI), 2,3-dimethyl-6-nitro-1H-indole (2,3,6-DMNI), and 4-nitro-1H-indole (4-NI)] (Figure 1) were synthesized and demonstrated for the first time to function as new dual-polarity MALDI matrices with broad applications. Analysis with standard compounds and complex mixtures demonstrated that NI matrices effectively detect positive and negative ions of metabolites, lipids, peptides, proteins, glycans, oligonucleotides, polymers, and environmental pollutant polyfluoroalkyl substances. The wide-range matrix applicability helps simplify matrix choices during MALDI MS and imaging sample preparation and enhances the detection sensitivity in complex mixture analysis. As slight indole ring substitution variations led to distinct matrix performance changes, nitro indole could function as a sensitive and versatile design platform for new matrix engineering.

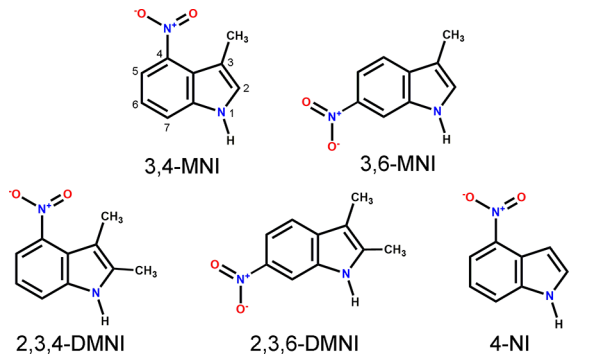

Figure 1. Chemical structures of the NI matrices.

EXPERIMENTAL SECTION

Materials. Chemicals for mass spectrometry analysis: peptide and protein calibration standards, 2,5-dihydroxybenzoic acid (DHB), alpha-cyano-4-hydroxylcinnamic acid (CHCA), and sinapinic acid (SA) were obtained from Bruker Daltonics (Billerica, MA, USA). 1,5-DAN, 9-aminoacridine (9-AA), L-α-phosphoinositols (PI) *Glycine max* (soy), fibrinopeptide B (fibB), ProteoMass Cytochrome c MALDI MS standard, beta-casein (b-CN), bovine serum albumin (BSA), Lacto-N-difucohexaose I (LNDFHI), perfluorooctanesulfonic acid (PFOS), and diammonium hydrogen citrate (dahc) were purchased from Sigma-Aldrich (St. Louis, MO, USA). Phosphocholine (PC) 16:0/16:0, phosphoethanolamine (PE) 16:0/18:1, and phosphatidate (PA) 16:0/18:1 were purchased from Avanti Polar Lipids (Alabaster, AL, USA). Eggs, bovine vitamin D whole milk, and frozen organic blueberries were purchased from a local grocery. All the other reagents, solvents, and salts were obtained from VWR International (Radnor, PA, USA).

Synthesis and Characterization. 3,4-MNI, 3,6-MNI, 2,3,4-DMNI, 2,3,6-DMNI, and 4-NI (Figure 1) were synthesized following ref 36. ^{1}H nuclear magnetic resonance spectroscopy (NMR) was performed on a Bruker DRX 400 MHz instrument, and high-resolution electrospray ionization (ESI) mass spectra were acquired on a Waters Xevo G2-XS Qtof mass spectrometer. The UV−vis spectra were recorded with a VWR UV-3100PC spectrophotometer.

Sample Preparation. *Matrix Performance with Standard Compounds.* The detection sensitivity test standards include PC 16:0/16:0, PE 16:0/18:1, and PA 16:0/18:1 at 10, 1, 0.1, 0.01 0.001 μM in methanol, PI *Glycine max* at 10, 1, 0.1, 0.01 0.001 ppm in methanol, fibB at 10, 1, 0.1, 0.01 0.001 μM in Milli-Q (MQ) water, BSA and b-CN at 10, 1, 0.1, 0.01 0.001 μM in 5 mM dahc ACN/water 1/1 and in MQ water, LNDFHI at 10, 1, 0.1, 0.01 0.001 μM in MQ water, and PFOS at 10, 1, 0.1, 0.01 0.001 ppm in MQ and in tap water. 3,4-MNI, 3,6-MNI, 2,3,4-DMNI, 2,3,6-DMNI, 4-NI, CHCA, DHB, 9-AA, 1,5-DAN, and SA matrices were prepared at 5 mM in ACN/water 1/1 0.1% TFA for fibB, at 25 mM in ACN/water 1/1 0.1% TFA for BSA and b-CN analysis, and at 1 or 5 mM in methanol for other analysis. A 1 μL portion of matrix was applied onto a Bruker Anchorchip target and dried, followed by 1 μL of standard solution applied on top. For BSA and b-CN protein analysis, samples and matrix were also mixed at 1.5:5 volume ratio, with 1 μL applied to the Anchorchip target. Sample spot homogeneity was evaluated with scanning imaging microscopy (SEM, SU3500, Hitachi) and Epson Perfection V600 photo scanner.

PFOS Quantitation in Water and Salt Tolerance. Calibration and verification standards were prepared in MQ water (0, 0.05, 0.1, 0.5, 1, 2, 5, and 10 ppb) and lab tap water (0, 0.05, 0.1, 0.5, 1, 2, 5, 10, 20, and 50 ppb) with 10 ppb of $^{13}C_8$−PFOS internal standard (IS) through isotopic dilution. Polypropylene centrifuge tubes and pipette tips were used to prevent background PFOS contamination. A 1 μL sample of 3,4-MNI (1 mM in methanol) was applied to an Anchorchip target and dried. A 3 μL portion of the standard solution was applied on top and dried. For salt tolerance study, 10 ppb PFOS solution was prepared in tap water with 0, 100 mM, 500 mM, and 1 M sodium chloride.

Egg Lipids Analysis. The lipid extraction followed the literature procedure:[11] 1.0 mL methanol and 0.5 mL chloroform were added to 400 μL of homogenized egg (yellow and white) and sonicated for 5 min. After addition of 0.5 mL of water and 0.5 mL of chloroform, the mixture was sonicated again for 5 min and centrifuged for 10 min at 7000 rpm, and the organic phase layer at the bottom was collected. 50 mM DHB, 1,5-DAN, 9-AA, and NI matrices in methanol was mixed with lipid extract 2:1 v/v, with 1 μL applied to a Bruker MTP Anchorchip target.

Milk Proteins Analysis. Bovine vitamin D whole milk was diluted 1/100 in MQ water or 5 mM dahc ACN/water (1/1). A 1 μL sample of the diluted milk was spotted on Anchorchip target and dried, with 1 μL of matrix solution (25 mM in ACN/water 1/1, 0.1% TFA) applied on top, or the sample was mixed with matrix at 1:4 volume ratio. Tested matrix solutions included 3,4-MNI, SA, CHCA, DHB, and 1,5-DAN.

Blueberry Extract and Tissue Imaging. One thawed frozen organic blueberry (~2 g) was crushed and sonicated in 2 mL of methanol for 30 min. The resulting methanol solution was centrifuged (10 min at 7000 rpm), and the supernatant was collected. A 1 μL sample of 3,4-MNI, 3,6-MNI, 2,3,4-DMNI, 2,3,6-DMNI, 4-NI, 1,5-DAN, 9-AA, and DHB (1 or 5 mM in methanol, or 25 mM in ACN/water 1/1 0.1% TFA) was spotted

https://doi.org/10.1021/acs.analchem.3c04684
Anal. Chem. 2024, 96, 1668−1677

Table 1. Detection Sensitivity Comparison of NI Matrices with Common Matrices in Positive (+) and Negative Ion (−) Mode[a]

Standards	3,4-MNI	3,6-MNI	2,3,4-DMNI	2,3,6-DMNI	4-NI	CHCA	DHB	9-AA	1,5-DAN	SA
PC 16:0/16:0 (+)	0.1	0.01	0.1	0.1	1	1	0.01	0.1	1	1
PE 16:0/18:1 (-)	0.1	1	0.1	1	1	10	10	0.1	0.1	10
PA 16:0/18:1 (-)	1	1	0.1	0.1	x	x	10	0.01	1	10
PI Glycine Max (-)	0.1	1	0.1	0.1	0.1	1	1	0.01	1	1
Peptide FibB (+)	0.01	0.1	10	10	0.1	0.01	0.01	1	0.01	0.1
Peptide FibB (-)	0.01	0.1	1	0.1	0.1	0.1	1	10	0.01	1
Glycan LNDFHI	0.1	0.1	10	1	x	1	0.1	10	10	10
Protein BSA (+)	1	0.1	x	x	x	1	1	x	10	1
Protein b-CN (+)	10	x	x	x	x	10	10	x	x	10
PFOS in tap water (-)	0.01	0.01	0.01	0.1	0.1	0.1	x	0.01	0.1	0.1
PFOS in water (-)	0.001	0.01	0.01	0.01	0.01	0.01	x	0.001	0.1	0.01

[a]PFOS and PI were tested at 10, 1, 0.1, 0.01, 0.001 ppm. All other compounds were tested at 10, 1, 0.1, 0.01, 0.001 μM, and the lowest concentration with S/N $\geq$ 5 was recorded (×: S/N < 5 at examined concentrations).

onto the Anchorchip target, and 1 μL of blueberry methanol extract was applied on top. For MALDI imaging, blueberries were stored at −20 °C and cut into 40 μm slices with a cryomicrotome (Tissue Tek II, Miles). The cut slices were thaw-mounted onto an ITO slide presprayed with 10 mM 2,3,6-MNI in methanol (3 × 1 mL to cover the whole ITO slide) using a Testors Aztek airbrush. The resulting tissue-mounted slide was dried in a desiccator for 30 min and subsequently stored at −20 °C in a sealed container. Prior to the imaging experiment, 1 mL of 10 mM 2,3,6-MNI in methanol was sprayed over the blueberry tissue area. For airbrush spray, the compressed air pressure was 20 psi, and the distance between the slide and the sprayer tip was ∼15 cm. Phosphorus red water suspension (1 μL) was applied on a control blueberry tissue of the same cut on the same ITO slide for mass calibration.

Matrix Vacuum Stability Measurements. The vacuum stability of NI matrices was measured in air using a quartz crystal microbalance (QCM). Briefly, 10 μL of a 50 mM matrix solution in ACN/water (85/15) was applied onto the gold-coated surface of a quartz crystal electrode and dried. The crystals were secured between two stainless steel plates (top plate with cutouts, connected with screws) fitted to a MALDI imaging slide holder and placed in the MALDI vacuum chamber. QCM oscillation frequencies were measured without matrix (f0), with matrix deposition before vacuum (f1), and with matrix deposition after 4 h vacuum (f2). The deposited matrix masses (a sum of matrix and residual solvents) were calculated by (f0 − f1) Hz × 20 ng/Hz. The mass loss after 4 h of vacuum was calculated by (f1 − f2) Hz × 20 ng/Hz, and the percentage of loss was calculated by (f2 − f1)/(f0 − f1).

MALDI MS/Imaging and ESI HRMS. The MALDI MS, collision-induced dissociation (CID, Argon collision gas 1.0 bar) MSMS, and imaging experiments were performed on a Bruker Daltonics rapifleX mass spectrometer equipped with a smart beam 3D laser (355 nm Nd:YAG, ≥100 μJ/pulse). For matrix comparison experiments, the MS spectra were acquired at optimum laser power for each matrix.

MS calibrations below m/z 4000 were performed with phosphorus red/CHCA matrix in positive and negative ion modes, and in the range of m/z 4000−100000 positive ion mode calibration was performed with Cytochrome c and BSA protein standards mixed with SA matrix. BSA, b-CN, and milk protein spectra were acquired in linear mode, and all other experiments were acquired in reflectron mode. The acquired MS and MSMS spectra were analyzed with flexAnalysis 4.0.

Blueberry metabolites/lipids MALDI imaging experiments were acquired in reflectron positive and negative ion modes with 50 μm laser spot size, 51% absolute laser power in negative ion mode, and 44% absolute laser power in positive ion mode, a raster width of 110 μm, number of scans of 2500, and laser frequency of 5000 shots per second. The imaging data was acquired with Bruker flexControl 4.0 and flexImaging 5.0 software and analyzed with Bruker SCILS Lab (Version 2023a Core). The optical images of the ITO slides were scanned with an Epson Perfection V600 photo scanner. For blueberry metabolites/lipids identification, MALDI TOF/TOF CID MSMS experiments were performed on selected ions in the extract and on tissue. ESI HRMS of the blueberry extract was performed on a Waters Xevo G2-XS Qtof instrument and analyzed with Masslynx 4.1 software. Metabolites' accurate masses and MALDI MSMS spectra were searched against databases such as FooDB,[37] HMDB,[38] and LIPID MAPS.[39]

RESULTS AND DISCUSSION

NI Synthesis and Characterization. NI matrices were synthesized and purified according to the patented procedures for modulators of ATP-binding cassette transporters.[36] The compound identity was confirmed by ^{1}H NMR chemical shifts (in $CDCl_3$ at 298 K) and ESI HRMS (Figures S1-1 to S1-5). All five NI matrices had efficient absorption at MALDI laser wavelength 355 nm, and the absorbance from high to low was $A_{2,3,6\text{-DMNI}} = 0.1855$, $A_{3,6\text{-MNI}} = 0.1787$, $A_{3,4\text{-MNI}} = 0.1706$, $A_{4\text{-NI}} = 0.1203$, and $A_{2,3,4\text{-DMNI}} = 0.1049$. The $A_{2,3,6\text{-DMNI}}$, $A_{3,6\text{-MNI}}$, and $A_{3,4\text{-MNI}}$ values were higher than the absorbance of common matrices examined ($A_{9\text{-AA}} = 0.0721$, $A_{\text{DHB}} = 0.0722$, $A_{1,5\text{-DAN}} = 0.0773$, and $A_{\text{SA}} = 0.1468$) except for CHCA ($A_{\text{CHCA}} = 0.6850$) (Figure S2).

Detection Sensitivity, Homogeneity, Vacuum Stability, and Ionization Mechanism. The detection sensitivity values of nitro indole matrices 3,4-MNI, 3,6-MNI, 2,3,4-DMNI, 2,3,6-DMNI, and 4-NI were compared with common matrices DHB, CHCA, SA, 1,5-DAN, and 9-AA for lipids (PC 16:0/16:0, PE 16:0/18:1, PA 16:0/18:1, PI *Glycine max*), peptide fibB, proteins (BSA and b-CN), glycan LNDFHI, and PFOS at

https://doi.org/10.1021/acs.analchem.3c04684
Anal. Chem. 2024, 96, 1668−1677

concentration range 0.001−10 μM or ppm (Table 1, Figures S3-1 to S3-3). (1) Lipids: 3,6-MNI and DHB had the highest sensitivity for PC 16:0/16:0 $[M + H]^+$ and $[M + Na]^+$ cations (0.01 μM), 4-NI, CHCA, 1,5-DAN, and SA had the lowest sensitivity (1 μM), and other matrices were intermediate (0.1 μM). 3,4-MNI, 2,3,4-DMNI, 9-AA, and 1,5-DAN were best for PE 16:0/18:1 $[M - H]^-$ anions (0.1 μM), with CHCA, DHB, and SA being the least sensitive (10 μM). PA 16:0/18:1 $[M - H]^-$ anions were detected at 0.01 μM with 9-AA; at 0.1 μM with 2,3,4-DMNI and 2,3,6-DMNI; at 1 μM with 3,4-MNI, 3,6-MNI, and 1,5-DAN; and at 10 μM with DHB and SA and was not detected by CHCA and 4-NI. PI *Glycin max* $[M - H]^-$ anions were detected at 0.01 ppm with 9-AA, at 0.1 ppm with 3,4-MNI, 2,3,4-DMNI, 2,3,6-DMNI, 4-NI, and at 1 ppm with the others. (2) Peptide/protein/glycan analysis: 3.4-MNI, CHCA, DHB, and 1,5-DAN were the most sensitive for fibB peptide $[M + H]^+$ cations and 3,4-MNI, 1,5-DAN most sensitive for $[M - H]^-$ anions (0.01 μM). For BSA protein $[M + H]^+$ and $[M + 2H]^{2+}$ ions, 3,6-MNI was the most sensitive (0.1 μM) and 3,4-MNI, CHCA, DHB, and SA intermediate (1 μM). 3,4-MNI, CHCA, DHB, and SA were effective for b-CN $[M + H]^+$ and $[M + 2H]^{2+}$ ions (10 μM), and 3,4-MNI, 3,6-MNI, and DHB were better for the LNDFHI glycan $[M + Na]^+$ analysis (0.1 μM). (3) PFOS: in MQ water, 3,4-MNI and 9-AA gave the best sensitivity (0.001 ppm) for the $[M - H]^-$ anions; other NI matrices showed similar performance as CHCA and SA (0.01 ppm), while DHB had matrix ion interference. In complex solutions such as tap water, 3,4-MNI, 3,6-MNI, 2,3,4-DMNI, and 9-AA maintained good sensitivity (0.01 ppm), while CHCA and SA sensitivity dropped to 0.1 ppm. In summary, 3,4-MNI demonstrated the best overall sensitivity for all compounds examined, while the other NI matrices showed a high sensitivity for various compounds. Table 1 also correlated the distinct performance shifts of NI matrices with indole ring substitution variations, such as with/without methyl groups and the position of the methyl and nitro groups, indicating that the nitro indole framework could function as a sensitive and versatile platform for new matrix designs.

SEM and photo scanned images (Figure S4) of sample spots on Anchorchip target demonstrated that 3,4-MNI, 3,6-MNI, 2,3,6-DMNI, and CHCA had more homogeneous and reproducible crystalline formation compared to 2,3,4-DMNI, 4-NI, DHB, 9-AA, 1,5-DAN, and SA. The 3,4-MNI and 3,6-MNI crystalline patterns changed dramatically based on solvent and sample choices, indicating the efficient and versatile matrix−sample interactions, correlating with their detection sensitivity for a wide variety of compounds.

MALDI matrix vacuum stability information is useful for MALDI MS and imaging experiments on high vacuum instruments and can be measured by a semimicro analytical balance.[15,40] QCM is a sensitive mass balance capable of measurement of nanogram to microgram mass changes. The piezoelectric thin quartz disk plated by gold electrodes oscillates at a defined frequency under electric potential and undergoes frequency change with addition or removal of mass (~20 ng/Hz).[41] QCM has been applied in MALDI to determine neutral particle yield and matrix desorption as a function of elevated temperature.[42,43] In this study, NI matrices were spotted on gold-plated quartz crystal electrodes, and the oscillation frequencies were measured. The results (Table S1) show that at 2.6×10^{-7} mbar after 4 h, 3,4-MNI and 3,6-MNI were the least stable with 76.5% and 77.8% mass loss, respectively; 4-NI was most stable (29.5% loss), while 2,3,4-MNI (33.7% loss) and 2,3,6-DMNI (53.2%) had an intermediate mass loss. RSD% of three measurements seemed to correlate with the matrix crystallization homogeneity (less surface area variation, Table S-1, Figure S5), with RSD less than 5% for the more homogeneous 3,4-MNI and 3,6-MNI matrix.

The effectiveness of NI MALDI matrices is related to the structural combination of the electron-rich indole ring with C4/C6 nitro and C2/C3 methyl substituents. The effect of methyl and nitro substituents on indole proton affinity (PA) has been reported.[44,45] Among the unsubstituted indole ring positions (N1, C2−C7, Figure 1), the C3 site has the highest proton affinity (922.5 kJ/mol) and N1 has the lowest (866.6 kJ/mol), which explains the well-known protonation preference of indole at the C3 site.[44] Methyl substituent releases electron density and increases PA for all positions except for the ipso one. Nitro substituent withdraws electrons and decreases PA values for all indole ring positions.[44] The sum effect is that multiple sites are available for protonation and deprotonation, which may contribute to the superb dual-polarity ionization efficiency of the NI matrices.

NI matrix background ions observed included monomeric or multimeric matrix cations and anions, such as $[m + H]^+$, $m^{+\bullet}$, $[m - H]^+$, $[m + Na]^+$, $[m + K]^+$, $[2m + H]^+$, $[2m - H]^+$, $[3m - H]^+$ and $[m - H]^-$, $[m - 2H]^-$, $[m - 3H]^-$, $[2m - H]^-$, $[2m - 3H]^-$, $[2m - 5H]^-$, and $[3m - 5H]^-$. The loss/gain of O and loss of NO from $[m - H]^-$, $[2m - 3H]^-$, and $[3m - 5H]^-$ are related to the aromatic nitro group (Figures S6-1 to S6-5).[46] The $[m - H]^+$ ions are not commonly observed in MALDI ionization but have been reported for some secondary and tertiary amines.[27,47,48] The proposed mechanisms include (1) matrix protonation $[m + H]^+$ followed by loss of H_2, (2) hydrogen atom transfer from $m^{+\bullet}$, and (3) hydride abstraction from neutral matrix molecules.[47] Considering the conjugated indole ring structure of NI, mechanism 1 seems less likely, while mechanisms 2 and 3 are possible. Dimeric cations $[2m - H]^+$ could be noncovalent attachment of m with $[m - H]^+$ or protonation of the covalently linked dimer with 2H loss, $[2m - 2H + H]^+$. Anions $[2m - 3H]^-$, $[2m - 5H]^-$, and $[3m - 5H]^-$ could be hydrogen loss from the covalently bonded dimers or trimers as $[2m - 2H - H]^-$, $[2m - 4H - H]^-$, and $[3m - 4H - H]^-$. Solvent choices did not affect the ion species identified in the NI matrix MS spectra, but the ACN/H_2O combination induced higher multimeric matrix ions than the methanol solvent. Matrix radical ions were minor compared to $[m + H]^+$/$[m + H - NO]^+$ or $[m - H]^-$, and analyte ionization may mainly follow the matrix analyte proton transfer mechanism.[8,9] The presence of $[m + Na]^+$ and $[m + K]^+$ ions suggested a possible matrix analyte cation transfer. Observed analyte ions for standards tested in Table 1 included $[M - H]^-$, $[M + H]^+$, $[M + 2H]^{2+}$, and $[M + Na]^+$. Additionally, NI matrices were tested effective for short chain oligonucleotide anions ($[M - H]^-$, $[M - 2H + K]^-$, $[M - 2H]^{2-}$, $[M - 3H + K]^{2-}$) and polymer $[M + Na]^+$ and $[M + Ag]^+$ cations (example spectra with 3,4-MNI matrix provided in Figures S7-1, S7-2). For proteins, ammonium salts enhanced analyte protonation by reducing analyte sodium ion binding.

Complex Mixture Analysis. *Direct PFOS Quantitation in Tap Water.* PFOS is one of the primary per- and poly fluoroalkyl substances (PFASs) that are linked to harmful health effects and persist in the environment (water, soil, and food chains).[49,50] PFOS quantitative analysis in complex mixtures is routinely performed with liquid chromatography (LC)-MS/MS. With multiple reaction monitoring (MRM) on tandem quadrupole

https://doi.org/10.1021/acs.analchem.3c04684
Anal. Chem. 2024, 96, 1668−1677

instruments, the typical instrument limit of quantitation (LOQ) is ~0.5 ppb.[51,52] Lower LOQ can be achieved with high-resolution (HR) MS precursor ion accurate mass, e.g., 0.05 ppb with Qtof MS[E53] and 0.025 ppb (method LOQ 0.1 ppt multiplied by SPE enrichment factor 250x) with orbitrap parallel reaction monitoring (PRM).[54] Combined with solid phase extraction (SPE), the methods LOQ could reach ppt and sub-ppt levels for both MRM and HRMS meathods.[54−56]

Compared to the LC-MS/MS platform, MALDI MS and imaging is an emerging technique that potentially allows direct PFAS analysis in complex mixtures,[57−60] with additional benefits of high throughput, minimal solvent consumption, and spatial distribution information on tissues. The challenge is finding the optimum matrix substances that are complex mixture-tolerant with good sensitivity/reproducibility. PFOS MALDI MS quantitation with 1,8-bis(tetramethylguanidino)-naphthalene[59] and desorption/ionization on porous silicon (DIOS)[60] as matrices were reported for SPE-treated tap water, but direct PFOS analysis in tap water with MALDI has not been reported to our knowledge.

Figure 2a,b compares the 3,4-MNI MALDI PFOS calibration curves and SEM images in MQ water versus in tap water. In MQ water, six PFOS concentration levels (0.05, 0.1, 0.5, 1, 2, and 10 ppb) with 10 ppb $^{13}C_8$−PFOS IS were spotted onto an Anchorchip target in six replicates. Peak area ratios of PFOS [M − H]$^-$ m/z 498.99 and $^{13}C_8$−PFOS [M − H]$^-$ m/z 507.02 were plotted versus their concentration ratios. For the linear range of 0.05−10 ppb, the regression coefficients were 0.9983, the average relative standard deviation was 5%, and the verification concentration of 5 ppb had a calculated value of 4.84 ppb (3.2% error) and an RSD of 4% (Table S2-1). In tap water, six PFOS concentration levels (0.5, 1, 2, 10, 20, and 50 ppb) with 10 ppb $^{13}C_8$−PFOS IS were spotted onto an Anchorchip target in six replicates. For the linear range of 0.5−50 ppb, the regression coefficients were 0.9982, the average relative standard deviation was 4%, and the verification concentration of 5 ppb had a calculated value of 5.25 ppb (5.0% error) and an RSD of 3% (Table S2-2). SEM images (Figure 2a,b) revealed that 3,4-MNI formed microscopic needle-shaped crystals over the hydrophilic anchor areas on the Anchorchip target. This crystallization pattern was reproducible from spots to spots in MQ water or tap water, demonstrating efficient sample matrix interaction and thus robust quantitative measurements.

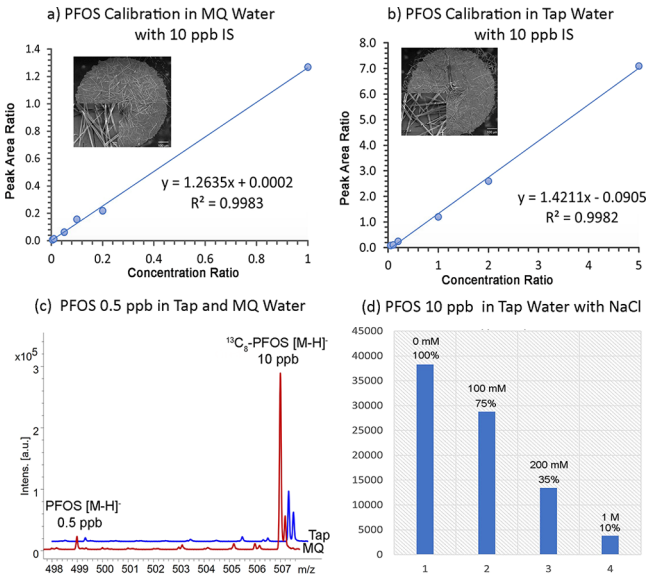

Figure 2. PFOS MALDI MS quantitation acquired with 10 ppb $^{13}C_8$−PFOS IS and 3,4-MNI matrix in negative ion mode: (a) MQ water PFOS calibration curve (0.05−10 ppb) and SEM image of the MQ water PFOS 10 ppb sample spot; (b) tap water PFOS calibration curve (0.5−50 ppb) and SEM image of the tap water PFOS 10 ppb sample spot; (c) MS spectra comparison of PFOS 0.5 ppb in tap and MQ water; (d) tap water 10 ppb PFOS [M − H]$^-$ ion intensity comparison with NaCl at 0, 100 mM, 500 mM, and 1M.

The PFOS LOQ with 3,4-MNI in MQ water (0.05 ppb) was superior to that in tap water (0.5 ppb) due to ion suppression in tap water. Figure 2c showed the ion intensity difference for PFOS of 0.5 ppb with 10 ppb IS in tap water and in MQ water. Figure S8 compares the LOQ and zero concentration spectra. Note that the MQ water spectra were acquired at lower laser power to ensure adequate peak resolution so that both PFOS and IS ions were clearly resolved from the background noise peaks, which was critical for accurate peak area integration. Salt tolerance of the 3,4-MNI matrix for PFOS analysis was evaluated by the optimum spectra comparison of 10 ppb PFOS in tap water with 0, 100, 200, and 1 M NaCl (Figure 2d). The peak area of m/z 498.99 [M − H]$^-$ declined to 75% (100 mM), 35% (500 mM), and 10% (1 M) compared with no NaCl added (Figure 3b), suggesting good salt tolerance of 3,4-MNI at the medium NaCl level (100 mM).

To summarize, direct MALDI MS analysis of PFOS in tap water with 3,4-MNI matrix demonstrated LOQ, precision, and accuracy comparable to standard LC-MS/MS MRM methods, with the additional benefits of complex mixture/salt tolerance, spped (acquisition time in seconds versus minutes per sample with LC-MS/MS), environmentally friendliness (minimal solvent consumption), and applicability for ppb level environmental contamination and environmental engineering PFOS analysis. PFOS analysis in MQ water had the LOQ (0.05 ppb) comparable to LC-MS/MS HRMS methods, which suggests when coupled to SPE enrichment this method is applicable to subppt level detection in drinking water. In addition, this method is suitable for automation and high throughput as the matrix was prespotted on a 384-spot target before sample spotting, and automatic target movement (smart complete) was applied during signal averaging.

Milk Protein and Egg Lipid Analysis. Milk is an important nutritional source of lipids, proteins, amino acids, vitamins, and minerals.[61] Proteins make up on average 3.5% of bovine milk, with 80% caseins and 18% whey proteins. Caseins are a family of related phosphoproteins with five types (aS1-CN, aS2-CN, b-CN, k-CN, and g-CN) and over 50 naturally occurring variants. Major whey proteins include beta-lactoglobin (bLG), alpha-lactalbumin (aLA), BSA, and immunoglobulins (Igs).[62] Diluted bovine vitamin D whole milk (without the fat and cell debris removal centrifugation step[63]) was chosen to evaluate 3,4-MNI performance for proteins in complex mixtures. Figure 3a compares the MS spectra acquired with 3,4-MNI, CHCA, 1,5-DAN, DHB, and SA matrices in positive ion mode. The protein ions observed were tentatively assigned based on reported milk protein molecular weights:[62] 24 KDa/12 KDa (singly/doubly charged) as b-CN, 23.6 KDa/11.8 KDa as αS1-CN, 18 KDa/9 KDa as bLG, and 14 KDa/7 KDa as aLA. In Figure 3a and inset, 1,5-DAN and CHCA failed to detect the singly charged b-CN ions (24 KDa), and the doubly charged ions were weak; SA and DHB produced singly and doubly charged b-CN ions but at weaker ion intensity compared to the 3,4-MNI matrix. 3,4-MNI

https://doi.org/10.1021/acs.analchem.3c04684
Anal. Chem. 2024, 96, 1668−1677

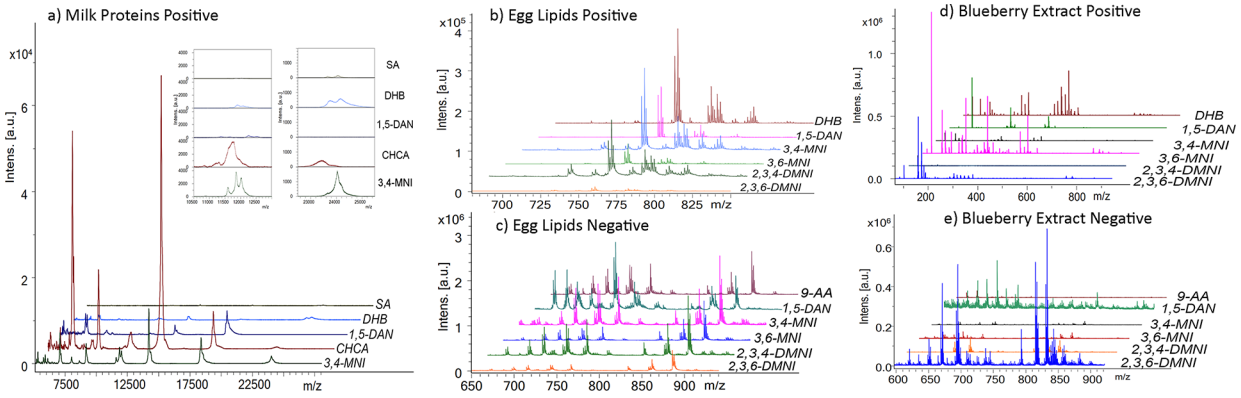

Figure 3. Matrix comparison MALDI MS spectra for milk proteins in positive ion mode (a), egg lipids in positive (b) and negative (c) ion modes, and blueberry extract in positive (d) and negative (e) ion mode.

showed a lower intensity of the singly charged αS1-CN ions but a higher intensity of the doubly charged ions compared to DHB and SA. CHCA was the most sensitive for aLA at 14 KDa/7 KDa. For the optimum detection sensitivity of all identified protein ions, 3,4-MNI was the best choice, least affected by ion suppression by complex milk constituents.

For lipid mixture analysis, egg lipid extract was selected to evaluate the performance of 3,4-MNI, 3,6-MNI, 2,3,4-DMNI, and 2,3,6-DMNI in comparison with common lipid MALDI matrices such as 9-AA for negative ions,[64] DHB for positive ions,[65] and 1,5-DAN for positive and negative dual-polarity ions.[13] (4-NI was not included due to its lower detection sensitivity for lipids in Table 1.) Sphingomyelin (SM) and PC ions in positive and PA, PE, and PI ions in negative ion mode were assigned based on reference reported assignments[11,66,67] and the MALDI TOF/TOF CID MSMS spectra (Table S3, Figures S9-1 to S9-7) in reference to general lipid MSMS fragmentation patterns.[68−72] Sn1 and Sn2 positions were not specified in the assignments as the ion abundance ratio is dependent on the headgroup, fatty acyl identity, and instrument conditions.[73,74] The egg lipid MALDI MS spectra matrix comparison (Figure 3b,c) demonstrated that 3,4-MNI, 3,6-MNI, 2,3,4-DMNI, and 2,3,6-DMNI all functioned as effective dual-polarity ion matrices, and 3,4-MNI had the best overall performance for positive and negative ions.

Blueberry Metabolites/Lipids Tissue Imaging. MALDI imaging is an emerging tool to visualize the distribution of a wide variety of plant metabolites across organs and tissues,[75,76] which is intrinsically challenging due to chemical complexity and potential ion suppression on tissues. DHB matrix has been applied to positive ion plant metabolites imaging, e.g., blueberry,[77] strawberry,[78,79] tomato,[80] and *Ginkgo biloba*.[81] In negative ion mode, 9-AA for tomato,[80] 1,5-DAN for strawberry,[82] 1,8-bisdimethyl-amino naphthalene (DMAN) for *Medicago truncatula*,[75] 2,4,6-trihydroxyacetophenone (THAP) for blueberry,[83] Michler's ethylketone for Chinese-yew seed,[84] and LDI (no matrix) for *Ginkgo biloba*[81] were reported. For blueberry metabolite imaging, reported studies were mostly limited to anthocyanins and polyphenols with DHB[77] or THAP[83] as a matrix.

In this study, NI matrix MALDI imaging applications in positive and negative ion modes for blueberry metabolites were investigated. Crude blueberry methanol extract was utilized to compare matrix performances of 3,4-MNI, 3,6-MNI, 2,3,4-DMNI, and 2,3,6-DMNI with DHB and 1,5-DAN in positive mode and with 9-AA and 1,5-DAN in negative mode (Figure 3d,e). In negative ion mode, 2,3,6-DMNI was the optimum matrix with intense ion signals and low matrix ion background (Figure 3e), while in positive ion mode, 3,6-MNI was the best performing NI matrix with ion patterns similar to those of the DHB matrix (Figure 3d). The unique advantage of NI matrices for blueberry metabolites seemed to be in the negative ion mode m/z 600−900 lipids region, where all four NI matrices demonstrate similar peak patterns with 2,3,6-DMNI the most intense, in contrast to no signal of 9-AA and noisy background of 1,5-DAN spectra, even though both matrices had good sensitivity with lipid standards (Table 1) and egg lipid extract (Figure 3c). To our knowledge, such enhancement of negative ions in the m/z 600−900 lipid region is unique for MALDI imaging of water-rich plant tissues. Unlike mammalian tissues, water-rich plant tissues are low in lipids with cell walls,[85] which could make MALDI imaging of lipids from such tissues more challenging, while reported plant lipid imaging studies were more focused on seeds (rich in lipids).[84,86]

Given its superior performance for the crude blueberry extract, 2,3,6-DMNI was then applied for blueberry tissue MALDI imaging. The 2,3,6-DMNI matrix formed monomer, dimer, trimer, and fragment ions at high concentrations and sublimed under the MALDI instrument vacuum (2.6×10^{-7} mbar) as demonstrated with the QCM volatility study. To reduce matrix ion background and minimize matrix sublimation effect, frozen blueberry tissue slices were mounted onto ITO slides precoated with a thin layer of 2,3,6-DMNI matrix, and then a second thin layer of matrix spray was applied over the blueberry tissue. The 2,3,6-DMNI matrix spray concentration (10 mM, 1.9 mg/mL) was much lower than the typical MALDI imaging matrix sprays, e.g. 50−150 mg/mL for DHB[75,77] and 15 mg/mL for DMAN.[75] The effectiveness of the 2,3,6-DMNI matrix at low concentration could be associated with its superior laser absorption at 355 nm (Figure S2, $A_{355\ nm\_2,34\text{-}DMNI} = 0.185$, $A_{355\ nm\_DHB} = 0.0722$). Applying an organic matrix layer under tissues shared some similarity with the nanostructure/nanoparticle layer under tissue method[87,88] in the order of matrix−tissue placement. As demonstrated by the control experiments (Figures S10 and S11), the matrix under and above the two-layer approach combined the ion desorption advantage of the matrix layer above and the vacuum stability advantage of the matrix layer under for optimum ion images.

Blueberry metabolites were putatively identified following mass-matching and MSMS-assisted identification rationales modified from ref 75. After TIC normalization, ions with higher intensity in blueberry skin/interior regions than the matrix-only

https://doi.org/10.1021/acs.analchem.3c04684
Anal. Chem. 2024, 96, 1668−1677

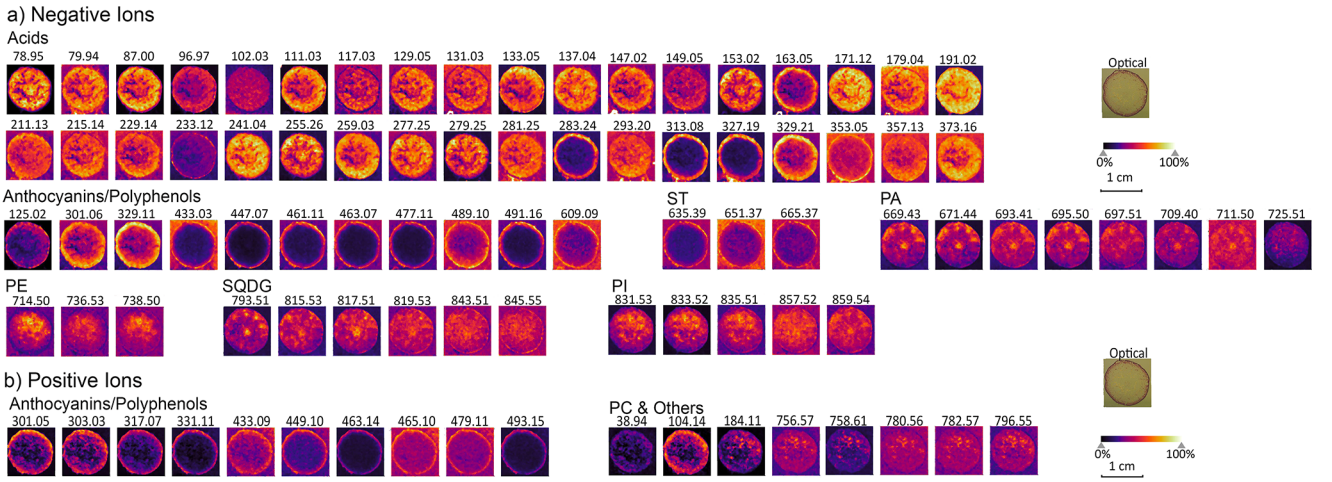

Figure 4. Blueberry metabolites/lipids MALDI imaging ion images acquired with 2,3,6-DMNI matrix in (a) negative and (b) positive ion mode, with *m*/*z* values listed above the images.

glass slide region (by region mean spectra and/or skyline spectra comparison) were considered promising metabolite masses, which were then compared with the blueberry crude extract Qtof ESI HRMS mass list, and the matching masses were identified if within <0.05 Da error. The matched Qtof HRMS accurate masses were then searched against databases (FooDB, HMDB, LIPID MAPS) and refs 75, 77, 83, 89, and 90 (<5 ppm mass accuracy typically). To further validate the assignments, MALDI CID MSMS spectra were collected for blueberry extract and on tissue. The results were similar, and the on-tissue CID spectra are provided in Figures SII-1 to SII-9 and compared with experimental/predicted LC-MSMS spectra in databases (FooDB, HMDB, LIPID MAPS) and/or MALDI MSMS spectra reported in references 75, 77, 83, 89, and 90. The Supporting Information Excel file lists the observed masses with MALDI MS imaging and Qtof HRMS, exact masses of the putatively identified compounds, and structurally informative CID MSMS fragment ions.

In negative ion mode, a total number of 72 metabolite ions (Figure 4a, Figures SII-1 to SII-7, and Supplemental Excel Table) were putatively identified with 2,3,6-DMNI matrix, including acids, anthocyanins/polyphenols, glycerophospholipids (PA, PE, PI), sulfoquinovosyldiacylglycerols (SQDG), and sterols (ST). The acids identified included phosphate *m*/*z* 78.95, sulfite *m*/*z* 79.94, monosaccharide phosphate *m*/*z* 259.03, aliphatic carboxylic acids (e.g., citric acid *m*/*z* 191.02, malic acid *m*/*z* 133.05, fatty acids *m*/*z* 255.26, 277.25, etc.), and aromatic carboxylic acids (e.g., coumarinic acid *m*/*z* 163.05, trans-5-O-caffeoyl-D-quinate *m*/*z* 353.05). In positive ion mode, 18 metabolite ions (Figure 4b, Figures SII-8 and SII-9, Supplemental Excel Table) were identified, e.g., potassium ions, anthocyanins/polyphenols, choline, phosphorylcholine, and PC.

Overall, the 2,3,6-DMNI matrix was demonstrated to be very effective for blueberry metabolites/lipids identification, especially in negative ion mode, and could be potentially useful for imaging applications for other plant types. The above−under tissue 2-layer matrix application method could be useful for other volatile matrices on high-vacuum MALDI instrument platforms. Note that matrix vacuum stability is not an issue for atmospheric pressure MALDI (AP-MALDI) which has become commercially more available on various instrument platforms (e.g., AP-MALDI-orbitrap,[91] AP-MALDI-QQQ,[92] and iM-Scope QT[93]) that are useful for vacuum-unstable small molecule analysis.

CONCLUSIONS

Five nitro indole derivatives (3,4-MNI, 3,6-MNI, 2,3,4-DMNI, 2,3,6-DMNI, and 4-NI) were synthesized and demonstrated to function as new dual-polarity positive and negative ion MALDI matrices with broad applications. Compared with common matrices DHB, CHCA, SA, 1,5-DAN, and 9-AA, 3,4-MNI demonstrated the best overall sensitivity for all standards examined (lipid, peptide, protein, glycan, and PFOS), while other NI matrices showed high sensitivity for various compounds. The five NI matrices were synthesized as part of a larger study, but they are commercially available.

For complex mixtures, the best overall detection sensitivity in comparison to common matrices was demonstrated by 3,4-MNI for egg lipids/milk proteins/PFOS in tap water and 2,3,6-DMNI for blueberry extract. Quantitative PFOS MALDI MS analysis with 3,4-MNI matrix demonstrated the LOQ (0.5 ppb in tap water, 0.05 ppb in MQ water, without SPE enrichment), accuracy, and precision comparable to the standard LC-MS/MS MRM method or HRMS method, with additional benefits of complex mixture/salt tolerance, ease of use, speed, high throughput, and minimal solvent consumption. With crystalline homogeneity (demonstrated by SEM and photo images) and general-purpose applications, 3,4-MNI could be potentially useful for MALDI quantitative analysis of a variety of molecules. 2,3,6-DMNI matrix was successfully applied for blueberry metabolites/lipids mapping, with a total of 90 negative or positive ions putatively identified which expanded the current knowledge base of plant MALDI imaging.

NI matrix showed various degrees of vacuum sublimation rate under high vacuum, as measured by matrix percentage loss after 4 h of vacuum treatment with a newly developed QCM method. However, the matrix vacuum sublimation did not affect routine MS analysis (e.g., 3,4-MNI PFOS quantitation), and a new matrix application method with thin 2,3,6-DMNI matrix layers under and above blueberry tissue allowed MALDI imaging success under high vacuum with a vacuum sublimation matrix. For increasingly more available AP MALDI instrumentation, matrix vacuum stability is not an issue.

In summary, NI matrices are demonstrated to be a unique family of MALDI matrices effective in positive and negative ion

https://doi.org/10.1021/acs.analchem.3c04684
Anal. Chem. 2024, 96, 1668−1677

modes with broad applications in many fields for qualitative and quantitative analysis. As demonstrated, slight substitution variations in the indole ring structure led to distinct matrix performance changes, which indicates that nitro indole could function as a sensitive and versatile design platform for new matrix engineering to further expand applications and solve analytical challenges. Work in preparation includes imaging applications for other plant and animal tissues, PFAS environmental analysis, and new NI matrix synthesis/characterization.

■ ASSOCIATED CONTENT

Supporting Information

The Supporting Information is available free of charge at https://pubs.acs.org/doi/10.1021/acs.analchem.3c04684.

NI compound ^{1}H NMR chemical shifts and UV−vis, detection sensitivity comparison, matrix/sample crystalline images, NI MALDI MS, oligonucleotide and polymer MALDI MS, QCM vacuum stability measurements, PFOS calibration statistics, egg lipids assignments and CID MSMS, blueberry tissue MS, and optical image comparison for matrix under and above (PDF)

Blueberry metabolites/lipids assignments and CID MSMS (PDF)

Observed masses with MALDI MS imaging and Qtof HRMS, exact masses of the putatively identified compounds, and structurally informative CID MSMS fragment ions (XLSX)

■ AUTHOR INFORMATION

Corresponding Authors

Qiaoli Liang − *Department of Chemistry & Biochemistry, The University of Alabama, Tuscaloosa, Alabama 35487, United States*; orcid.org/0000-0002-2395-8778; Email: liang005@ua.edu

Gayan B. Wijeratne − *Department of Chemistry & Biochemistry, The University of Alabama, Tuscaloosa, Alabama 35487, United States*; Email: gwijeratne@ua.edu

Authors

Pritam Mondal − *Department of Chemical Sciences, Indian Institute of Science Education and Research Mohali, Punjab 140306, India*; orcid.org/0000-0002-7071-1970

Qi Li − *Department of Chemical and Biological Engineering, The University of Alabama, Tuscaloosa, Alabama 35487, United States*

Tahir Maqbool − *Department of Civil, Construction and Environmental Engineering, The University of Alabama, Tuscaloosa, Alabama 35487, United States*

Chao Zhao − *Department of Chemical and Biological Engineering, The University of Alabama, Tuscaloosa, Alabama 35487, United States*

Daqian Jiang − *Department of Civil, Construction and Environmental Engineering, The University of Alabama, Tuscaloosa, Alabama 35487, United States*

Greg J. Szulczewski − *Department of Chemistry & Biochemistry, The University of Alabama, Tuscaloosa, Alabama 35487, United States*

Complete contact information is available at: https://pubs.acs.org/10.1021/acs.analchem.3c04684

Notes

The authors declare no competing financial interest.

■ ACKNOWLEDGMENTS

The authors gratefully acknowledge NSF CHE-1726812 from the Major Research Instrumentation Program for purchase of the MALDI/TOF-TOF mass spectrometer, and software technical support for SCILS Lab and flexImaging by Bruker. This work was supported by the National Science Foundation CAREER Award CHE-2045005 (to G.B.W.). C.Z. acknowledges support from the National Institute of General Medical Sciences of the National Institutes of Health under award number R01GM144388.

■ REFERENCES

(1) Tanaka, K.; Waki, H.; Ido, Y.; Akita, S.; Yoshida, Y.; et al. *Rapid Commun. Mass Spectrom.* **1988**, *2* (8), 151−153.

(2) Leopold, J.; Popkova, Y.; Engel, K. M.; Schiller, J. *Biomolecules* **2018**, *8* (4), 173.

(3) Pappin, D. J.; Hojrup, P.; Bleasby, A. J. *Curr. Biol.* **1993**, *3* (6), 327−332.

(4) Chaurand, P.; Stoeckli, M.; Caprioli, R. M. *Anal. Chem.* **1999**, *71* (23), 5263−5270.

(5) Harvey, D. J. *Mass Spectrom. Rev.* **2021**, *40* (4), 408−565.

(6) McLuckey, S. A.; Van Berkel, G. J.; Glish, G. L. *J. Am. Soc. Mass. Spectrom.* **1992**, *3* (1), 60−70.

(7) Montaudo, G.; Samperi, F.; Montaudo, M. S. *Prog. Polym. Sci.* **2006**, *31* (3), 277−357.

(8) Zenobi, R.; Knochenmuss, R. *Mass Spectrom. Rev.* **1998**, *17* (5), 337−366.

(9) Knochenmuss, R.; Zenobi, R. *Chem. Rev.* **2003**, *103* (2), 441−452.

(10) Calvano, C. D.; Ventura, G.; Cataldi, T. R.; Palmisano, F. *Anal. Bioanal. Chem.* **2015**, *407* (21), 6369−6379.

(11) Weißflog, J.; Svatoš, A. *RSC Adv.* **2016**, *6* (79), 75073−75081.

(12) Scott, A. J.; Flinders, B.; Cappell, J.; Liang, T.; Pelc, R. S.; Tran, B.; Kilgour, D. P.; Heeren, R. M.; Goodlett, D. R.; Ernst, R. K. *FEMS Pathog. Dis.* **2016**, *74* (8), ftw097.

(13) Dong, W.; Shen, Q.; Baibado, J. T.; Liang, Y.; Wang, P.; Huang, Y.; Zhang, Z.; Wang, Y.; Cheung, H.-Y. *Int. J. Mass spectrom.* **2013**, *343*, 15−22.

(14) Thomas, A. l.; Charbonneau, J. L.; Fournaise, E.; Chaurand, P. *Anal. Chem.* **2012**, *84* (4), 2048−2054.

(15) Li, B.; Sun, R.; Gordon, A.; Ge, J.; Zhang, Y.; Li, P.; Yang, H. *Anal. Chem.* **2019**, *91* (13), 8221−8228.

(16) Huang, P.; Huang, C.-Y.; Lin, T.-C.; Lin, L.-E.; Yang, E.; Lee, C.; Hsu, C.-C.; Chou, P.-T. *Anal. Chem.* **2020**, *92* (10), 7139−7145.

(17) Tang, W.; Gordon, A.; Wang, F.; Chen, Y.; Li, B. *Anal. Chem.* **2021**, *93* (26), 9083−9093.

(18) Kaushik, N. K.; Kaushik, N.; Attri, P.; Kumar, N.; Kim, C. H.; Verma, A. K.; Choi, E. H. *Molecules* **2013**, *18* (6), 6620−6662.

(19) Nielen, M. W.; Malucha, S. *Rapid Commun. Mass Spectrom.* **1997**, *11* (11), 1194−1204.

(20) Galesio, M.; Rial-Otero, R.; Capelo-Martínez, J. L. *Rapid Commun. Mass Spectrom.* **2009**, *23* (12), 1783−1791.

(21) Habumugisha, T.; Zhang, Z.; Ndayishimiye, J. C.; Nkinahamira, F.; Kayiranga, A.; Cyubahiro, E.; Rehman, A.; Yan, C.; Zhang, X. *Anal. Methods* **2022**, *14* (7), 763−772.

(22) Bai, J.; Liang, X.; Liu, Y. H.; Zhu, Y.; Lubman, D. M. *Rapid Commun. Mass Spectrom.* **1996**, *10* (7), 839−844.

(23) Nonami, H.; Fukui, S.; Erra-Balsells, R. *J. Mass Spectrom.* **1997**, *32* (3), 287−296.

(24) Nonami, H.; Tanaka, K.; Fukuyama, Y.; Erra-Balsells, R. *Rapid Commun. Mass Spectrom.* **1998**, *12* (6), 285−296.

(25) Nonami, H.; Wu, F.; Thummel, R. P.; Fukuyama, Y.; Yamaoka, H.; Erra-Balsells, R. *Rapid Commun. Mass Spectrom.* **2001**, *15* (23), 2354−2373.

(26) Yamagaki, T.; Nakanishi, H. *Glycoconj. J.* **1999**, *16* (8), 385−389.

(27) Nuutinen, J. M.; Purmonen, M.; Ratilainen, J.; Rissanen, K.; Vainiotalo, P. *Rapid Commun. Mass Spectrom.* **2001**, *15* (15), 1374−1381.

(28) Lloyd, P. M.; Suddaby, K. G.; Varney, J. E.; Scrivener, E.; Derrick, P. J.; Haddleton, D. M. *Eur. Mass Spectrom.* **1995**, *1* (1), 293−300.
(29) Choi, H.; Lee, D.; Kim, Y.; Nguyen, H.-Q.; Han, S.; Kim, J. *J. Am. Soc. Mass. Spectrom.* **2019**, *30* (7), 1174−1178.
(30) Asakawa, D.; Smargiasso, N.; De Pauw, E. *Anal. Chem.* **2012**, *84* (17), 7463−7468.
(31) Fukuyama, Y.; Izumi, S.; Tanaka, K. *Anal. Chem.* **2016**, *88* (16), 8058−8063.
(32) Fukuyama, Y.; Izumi, S.; Tanaka, K. *J. Am. Soc. Mass. Spectrom.* **2018**, *29* (11), 2227−2236.
(33) Steven, R. T.; Race, A. M.; Bunch, J. *J. Am. Soc. Mass. Spectrom.* **2013**, *24* (5), 801−804.
(34) Bonesi, S. M.; Mesaros, M.; Cabrerizo, F. M.; Ponce, M. A.; Bilmes, G. M.; Erra-Balsells, R. *Chem. Phys. Lett.* **2007**, *446* (1−3), 49−55.
(35) Tarzi, O. I.; Ponce, M. A.; Cabrerizo, F. M.; Bonesi, S. M.; Erra-Balsells, R. *Arkivoc* **2006**, *2005* (12), 295−310.
(36) Hadida Ruah, S. S.; Grootenhuis, P. D. J.; Van Goor, F. F.; Zhou, J.; Bear, B. R.; Miller, M. T.; McCartney, J.; Djamel Numa, M. M.; Yang, X.; Nair, N. US 20160271105A1, 2016.
(37) https://foodb.ca/ (accessed 2023-10-20).
(38) Wishart, D. S.; Feunang, Y. D.; Marcu, A.; Guo, A. C.; Liang, K.; Vázquez-Fresno, R.; Sajed, T.; Johnson, D.; Li, C.; Karu, N.; et al. *Nucleic Acids Res.* **2018**, *46* (D1), D608−D617.
(39) Fahy, E.; Sud, M.; Cotter, D.; Subramaniam, S. *Nucleic Acids Res.* **2007**, *35*, W606−W612.
(40) Yang, J.; Norris, J. L.; Caprioli, R. *J. Mass Spectrom.* **2018**, *53* (10), 1005−1012.
(41) O'sullivan, C.; Guilbault, G. *Biosens. Bioelectron.* **1999**, *14* (8−9), 663−670.
(42) Quist, A. P.; Huth-Fehre, T.; Sundqvist, B. U.; Vertes, A. *Rapid Commun. Mass Spectrom.* **1994**, *8* (2), 149−154.
(43) Wallace, W. E.; Arnould, M.; Knochenmuss, R. *Int. J. Mass Spectrom.* **2005**, *242* (1), 13−22.
(44) Otero, N.; González Moa, M. J.; Mandado, M.; Mosquera, R. A. *Chem. Phys. Lett.* **2006**, *428* (4), 249−254.
(45) Otero, N.; Mandado, M.; Mosquera, R. A. *J. Phys. Chem. A* **2007**, *111*, 5557−5562.
(46) Balasanmugam, K.; Viswanadham, S. K.; Hercules, D. M. *Anal. Chem.* **1983**, *55* (14), 2424−2426.
(47) Awad, H.; Stoudemayer, M.; Usher, L.; Amster, I.; Cohen, A.; Das, U.; Whittal, R.; Dimmock, J.; El-Aneed, A. *J. Mass Spectrom.* **2014**, *49* (11), 1139−1147.
(48) Kang, C.; Zhou, Y.; Du, Z.; Bian, Z.; Wang, J.; Qiu, X.; Gao, L.; Sun, Y. *J. Mass Spectrom.* **2013**, *48* (12), 1318−1324.
(49) Jahnke, A.; Berger, U. *J. Chromatogr. A* **2009**, *1216* (3), 410−421.
(50) Naidu, R.; Nadebaum, P.; Fang, C.; Cousins, I.; Pennell, K.; Conder, J.; Newell, C.; Longpré, D.; Warner, S.; Crosbie, N.; et al. *Environ. Technol. Innov.* **2020**, *19*, 100915.
(51) Yang, W.; Guo, J.; Dong, L.; Huang, Y. https://www.agilent.com/cs/library/applications/application-environmental-pfo-and-pfoa-ultivo-lctq-5994-0437en-agilent.pdf (accessed 2023-11-28).
(52) Xiang, L.; Sun, T.-F.; Chen, L.; Xiao, T.; Cai, Q.-Y.; Li, H.; He, D.-C.; Wong, M.-H.; Li, Y.-W.; Mo, C.-H. *Food Anal. Methods* **2017**, *10* (7), 2518−2528.
(53) Mullin, L.; Cleland, G. https://www.waters.com/webassets/cms/library/docs/720005727en.pdf (accessed 2023-11-28).
(54) Haghani, A.; Eaton, A.; Eaton, E.; CA, M.; Jack, R.; Bromirski, M. https://assets.thermofisher.com/TFS-Assets/CMD/Application-Notes/an-65499-lc-ms-epa-method-537-1-validation-an65499-en.pdf (accessed 2023-11-28).
(55) Ullah, S.; Alsberg, T.; Vestergren, R.; Berger, U. *Anal. Bioanal. Chem.* **2012**, *404*, 2193−2201.
(56) Al Amin, M.; Sobhani, Z.; Liu, Y.; Dharmaraja, R.; Chadalavada, S.; Naidu, R.; Chalker, J. M.; Fang, C. *Environ. Technol. Innov.* **2020**, *19*, 100879.
(57) Li, X.; Li, T.; Wang, Z.; Wei, J.; Liu, J.; Zhang, Y.; Zhao, Z. *Talanta* **2021**, *226*, 122150.
(58) Bian, Y.; He, M.-Y.; Ling, Y.; Wang, X.-J.; Zhang, F.; Feng, X.-S.; Zhang, Y.; Xing, S.-G.; Li, J.; Qiu, X.; et al. *Environ. Pollut.* **2022**, *293*, 118505.
(59) Cao, D.; Wang, Z.; Han, C.; Cui, L.; Hu, M.; Wu, J.; Liu, Y.; Cai, Y.; Wang, H.; Kang, Y. *Talanta* **2011**, *85* (1), 345−352.
(60) Kawasaki, H.; Shimomae, Y.; Watanabe, T.; Arakawa, R. *Colloids Surf., A* **2009**, *347* (1−3), 220−224.
(61) Haug, A.; Høstmark, A. T.; Harstad, O. M. *Lipids Health Dis.* **2007**, *6* (1), 25.
(62) Vincent, D.; Elkins, A.; Condina, M. R.; Ezernieks, V.; Rochfort, S. *PLoS One* **2016**, *11* (10), No. e0163471.
(63) Di Francesco, L.; Di Girolamo, F.; Mennini, M.; Masotti, A.; Salvatori, G.; Rigon, G.; Signore, F.; Pietrantoni, E.; Scapaticci, M.; Lante, I.; et al. *Nutrients* **2018**, *10* (9), 1238.
(64) Sun, G.; Yang, K.; Zhao, Z.; Guan, S.; Han, X.; Gross, R. W. *Anal. Chem.* **2008**, *80* (19), 7576−7585.
(65) Harvey, D. J. *J. Mass Spectrom.* **1995**, *30* (9), 1333−1346.
(66) Teuber, K.; Schiller, J.; Fuchs, B.; Karas, M.; Jaskolla, T. W. *Chem. Phys. Lipids* **2010**, *163* (6), 552−560.
(67) Wood, P. L.; Muir, W.; Christmann, U.; Gibbons, P.; Hancock, C. L.; Poole, C. M.; Emery, A. L.; Poovey, J. R.; Hagg, C.; Scarborough, J. H.; et al. *Poult. Sci.* **2021**, *100* (2), 887−899.
(68) Zhou, L.; Wang, Y.; Wang, X.; Liang, Y.; Huang, Z.; Zeng, X. *J. Agric. Food Chem.* **2017**, *65* (6), 1229−1238.
(69) Wang, Z.; Cai, Y.; Wang, Y.; Zhou, X.; Zhang, Y.; Lu, H. *Sci. Rep.* **2017**, *7* (1), 44466.
(70) Hsu, F.-F.; Turk, J. *J. Chromatogr. B* **2009**, *877* (26), 2673−2695.
(71) https://www.lipidmaps.org/resources/standards.php (accessed 2023-10-20).
(72) https://www.lipidmaps.org/resources/tools/ms (accessed 2023-10-20).
(73) Ekroos, K.; Ejsing, C. S.; Bahr, U.; Karas, M.; Simons, K.; Shevchenko, A. *J. Lipid Res.* **2003**, *44* (11), 2181−2192.
(74) Zhang, W.; Jian, R.; Zhao, J.; Liu, Y.; Xia, Y. *J. Lipid Res.* **2022**, *63*, 100219.
(75) Ye, H.; Gemperline, E.; Venkateshwaran, M.; Chen, R.; Delaux, P. M.; Howes-Podoll, M.; Ané, J. M.; Li, L. *Plant J.* **2013**, *75* (1), 130−145.
(76) Sturtevant, D.; Lee, Y.-J.; Chapman, K. D. *Curr. Opin. Biotechnol.* **2016**, *37*, 53−60.
(77) Yoshimura, Y.; Enomoto, H.; Moriyama, T.; Kawamura, Y.; Setou, M.; Zaima, N. *Anal. Bioanal. Chem.* **2012**, *403* (7), 1885−1895.
(78) Wang, J.; Yang, E.; Chaurand, P.; Raghavan, V. *Food Chem.* **2021**, *345*, 128838.
(79) Enomoto, H.; Sato, K.; Miyamoto, K.; Ohtsuka, A.; Yamane, H. *J. Agric. Food Chem.* **2018**, *66* (19), 4958−4965.
(80) Nakamura, J.; Morikawa-Ichinose, T.; Fujimura, Y.; Hayakawa, E.; Takahashi, K.; Ishii, T.; Miura, D.; Wariishi, H. *Anal. Bioanal. Chem.* **2017**, *409*, 1697−1706.
(81) Li, B.; Neumann, E. K.; Ge, J.; Gao, W.; Yang, H.; Li, P.; Sweedler, J. V. *Plant Cell Environ.* **2018**, *41* (11), 2693−2703.
(82) Enomoto, H. *Molecules* **2020**, *25* (20), 4600.
(83) Dare, A. P.; Günther, C. S.; Grey, A. C.; Guo, G.; Demarais, N. J.; Cordiner, S.; McGhie, T. K.; Boldingh, H.; Hunt, M.; Deng, C.; et al. *Food Chem.* **2022**, *374*, 131703.
(84) Shi, Y.; Hu, H.; Hao, Q.; Wu, R.; Wang, L.; Qin, L.; Gu, W.; Liu, H.; Jiang, D.; Hong, L.; et al. *Chem. Commun.* **2022**, *58* (5), 633−636.
(85) Liu, H.; Pan, Y.; Xiong, C.; han, J.; Wang, X.; Chen, J.; Nie, Z. *TrAC, Trends Anal. Chem.* **2022**, *157*, 116809.
(86) de Souza, L. P.; Borghi, M.; Fernie, A. *Int. J. Mol. Sci.* **2020**, *21* (23), 8987.
(87) Greving, M. P.; Patti, G. J.; Siuzdak, G. *Anal. Chem.* **2011**, *83* (1), 2−7.
(88) Iakab, S.-A.; Baquer, G.; Lafuente, M.; Pina, M. P.; Ramírez, J. L.; Ràfols, P.; Correig-Blanchar, X.; García-Altares, M. *Anal. Chem.* **2022**, *94* (6), 2785−2793.
(89) Bederska-Łojewska, D.; Pieszka, M.; Marzec, A.; Rudzińska, M.; Grygier, A.; Siger, A.; Cieślik-Boczula, K.; Orczewska-Dudek, S.; Migdał, W. *Molecules* **2021**, *26* (24), 7446.

(90) Forney, C. F.; Kalt, W.; Jordan, M. A.; Vinqvist-Tymchuk, M. R.; Fillmore, S. A. *J. Berry Res.* **2012**, *2* (3), 169−177.
(91) Mahale, V.; Singh, A.; Phadke, G. S.; Ghanate, A. D.; Oulkar, D. P.; Banerjee, K.; Panchagnula, V. *J. AOAC Int.* **2017**, *100* (3), 640−646.
(92) Bowman, A. P.; Sawicki, J.; Talaty, N. N.; Buck, W. R.; Yang, J.; Wagner, D. S. *Pharm.* **2022**, *15* (10), 1180.
(93) Islam, A.; Sakamoto, T.; Zhai, Q.; Rahman, M. M.; Mamun, M. A.; Takahashi, Y.; Kahyo, T.; Setou, M. *Pharm.* **2022**, *15* (11), 1314.

https://doi.org/10.1021/acs.analchem.3c04684
Anal. Chem. 2024, 96, 1668−1677